Journal of Geographic Information and Decision Analysis, vol. 2, no. 2, pp. 152 -167, 1998

Interpolation of Rainfall Data with Thin Plate Smoothing Splines - Part II: Analysis of Topographic Dependence

Michael F. Hutchinson
Centre for Resource and Environmental Studies, Australian National University, Canberra, ACT 0200, Australia
hutch@cres.anu.edu.au

ABSTRACT **Thin plate smoothing splines incorporating varying degrees of topographic dependence were used to interpolate 100 daily rainfall values, with the degree of data smoothing determined by minimizing the generalised cross validation. Analyses were performed on the square roots of the rainfall values. Model calibration was made difficult by short range correlation and the small size of the data set. Short range correlation was partially overcome by removing one point from each of the five closest pairs of data points. An additional five representative points were removed to make up a set of 10 withheld points to assess model error. Three dimensional spline functions of position and elevation, from digital elevation models of varying resolution, were used to assess the optimum scaling of elevation and an optimum DEM resolution of 10 km. A linear sub-model, depending on the two horizontal components of the unit normal to the scaled DEM, was used to form a five dimensional partial spline model which identified a south western aspect effect. This model also had slightly smaller estimated predictive error. The model was validated by reference to the prevailing upper atmosphere wind field and by comparing predictive accuracies on 367 withheld data points. Model selection was further validated by fitting the various spline models to the 367 data points and using the 100 data points to assess model error. This verified that there were small, but significant, elevation and topographic aspect effects in the data, when calculated from a 10 km resolution DEM, providing a physical explanation for the short range correlation identified by the two dimensional analysis in the companion paper.**

KEYWORDS: **partial thin plate smoothing splines, digital elevation model, topographic dependence, generalized cross validation, data smoothing, short range correlation, rainfall data, square root transformation.**

ACKNOWLEDGMENT The author gratefully acknowledges the assistance of Antoine Zelenka, Peter Zbinden and colleagues of the Swiss Meteorological Institute for their timely provision of rainfall statistics and synoptic data supporting this analysis.

Contents

---

1. Introduction and methodology

Rainfall, particularly at the daily time scale, typically displays complex spatial patterns. These are often related to topography and prevailing wind direction, but calibration of such factors can be difficult for several reasons. Precipitation usually displays a spatially varying dependence on elevation. Moreover, high altitude stations are small in number and measurements can be contaminated by measurement error associated with high wind speed and with snow (Barry 1981). Calibration is thus made even more difficult if the data set is small, as in the case investigated here.

This paper examines higher dimensional analyses of daily rainfall data, using thin plate smoothing splines, and partial thin plate smoothing splines, to incorporate varying degrees of topographic dependence. Partial thin plate splines, as described by Bates *et al.* (1987) and Wahba (1990), were obtained using the ANUSPLIN package (Hutchinson 1997a). Two, three, four and five dimensional spline models, as discussed by Hutchinson (1995a), are examined. The companion paper (Hutchinson 1998) uses thin plate smoothing splines to examine in detail two dimensional dependence of the same data. It identifies short range correlation structure in the data with a range less than 10 km. In keeping with the error analysis of the companion paper, the analyses described below were performed on the square roots of the observed rainfall data.

The companion paper also gives a brief introduction to thin plate smoothing splines and applications to climate analysis. It also describes the relationship of thin plate smoothing splines to kriging methods, as examined by Hutchinson (1993) and Hutchinson and Gessler (1994). Key features of thin plate smoothing spline analyses are their robustness and operational simplicity. An important diagnostic associated with thin plate smoothing spline analyses is the *signal* of the fitted spline, as estimated by the trace of the influence matrix. This gives the effective number of parameters of the fitted spline model. It should normally be less than about half of the number of data points. The companion paper shows that the relative signal can be used to assess short range correlation structure in the data.

2. Features of the rainfall data

Three features of the rainfall data set deserve attention, in addition to the features discussed in the companion paper. Firstly, as discussed above, the small size of the data set places limits on the complexity of analyses of topographic dependence.

Secondly, from the point of view of three dimensional spline analysis, errors in both position and elevation of the data points should be considered. A digital elevation model (DEM) with a spatial resolution of 1 km was provided. This DEM had been interpolated from a 30 second DEM in geographic coordinates calculated by the US Geological Survey (USGS). Lack of precision in horizontal coordinates, which have estimated standard error of around 1 km, translates into lack of precision in estimated station elevations, especially in areas of high relief such as the Swiss Alps. This was assessed by estimating station elevations from the original USGS DEM, using the geographic coordinates of the stations. Elevations were interpolated from the USGS DEM using biquadratic spline interpolation. The method of interpolation of elevations in the 1 km DEM is unknown. Elevations of the stations from the two DEMs are compared in Figure 1(a), showing positive and negative differences as large as 300 metres, and a root mean square difference of 100 metres.

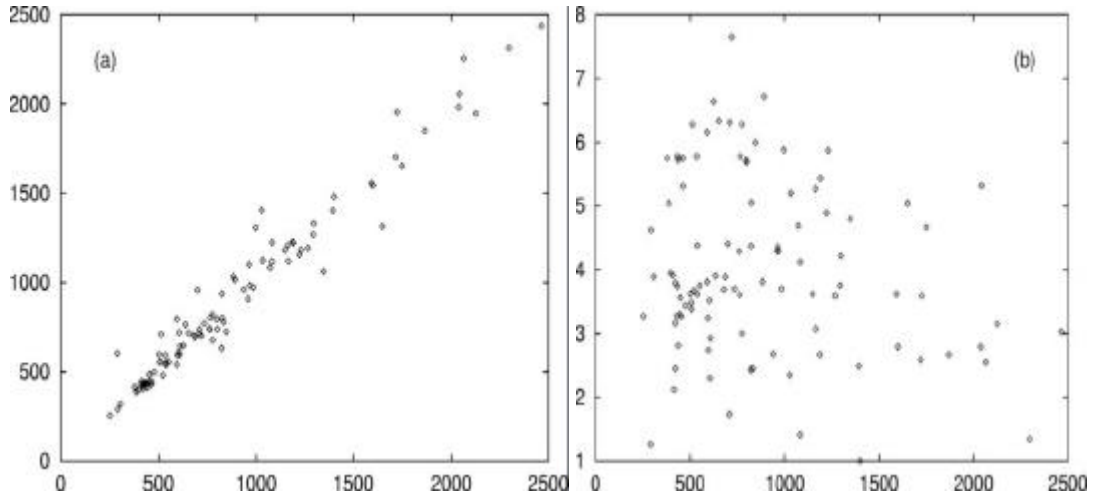

Figure 1 (a) Station elevation from the USGS 30 second DEM versus station elevation from the 1 km DEM ; (b) Square root rainfall ($mm^{1/2}$) versus station elevation from the 1 km DEM.

Thirdly, the data do not indicate simple dependence on elevation. This is shown clearly in Figure 1(b) where square root rainfall is plotted versus station elevation, as derived from the 1 km DEM.

3. Calculation of topographic variables

In view of the lack of horizontal and vertical precision of the data, and the likely coarse scale of elevation dependence of the precipitation data, the 1 km DEM was subjected to smoothing, to produce DEMs of successively coarser resolutions. These were calculated by supplying the 1 km DEM points as data for the ANUDEM elevation gridding program (Hutchinson 1996, 1997b). Data smoothing by ANUDEM, which improved representation of terrain slope and aspect, was adjusted for the number of data points per

output DEM grid cell. The resultant DEMs have elevations which are slightly smoothed local averages of the 1 km DEM elevations across each coarse resolution DEM grid cell. Summary statistics of the original and smoothed DEMs are listed in Table 1. The RMS slope rapidly declines as a function of resolution. The coarse resolution DEMs remove the ambiguity in station elevations shown in Figure 1(a). Station elevations for the ensuing analyses were obtained from each DEM using biquadratic spline interpolation.

Table 1. Summary statistics of the original 1 km DEM and the smoothed coarse resolution DEMs.

Resolution (km)	RMS Residual from 1 km DEM (m)	RMS Slope (%)	Mean Elevation (m)	Max Elevation (m)
1	0	21.8	1070	4469
2.5	171	10.4	1074	4023
5	242	5.8	1074	3473
8	292	3.7	1075	3127
10	315	3.1	1069	3151
20	381	1.8	1077	2925

Topographic slope and aspect effects on rainfall were modelled by using the eastern and northern components of the unit normal vector to the smoothed DEMs as predictor variables. These components are given respectively by

$$p = - z_x /(1 + z_x^2 + z_y^2)^{1/2} \quad (1)$$

$$q = - z_y /(1 + z_x^2 + z_y^2)^{1/2} \quad (2)$$

where z_x and z_y are the partial derivatives of the elevation surface $z(x, y)$ with respect to x and y. Equivalently

$$p = cos(a)\, sin(q) \quad (3)$$

$$q = sin(a)\, sin(q) \quad (4)$$

where, for each point on the DEM, a is the aspect angle, given by the direction of steepest slope, and q is the angle of steepest slope itself.

The variables p, q are *continuous* functions of position, with largest magnitude on steepest slopes, and reducing to zero on flat slopes in valley floors and on peaks. Using both p, q in the analysis permits the incorporation of the effects of both slope and aspect in a process oriented fashion. It also allows the *direction* of these effects to be determined without reference to the prevailing wind field.

4. Selection of withheld data

As in the two dimensional analysis in the companion paper, initial three dimensional thin plate smoothing spline analyses yielded exact interpolation, indicating short range correlation in the data. This occurred for station elevations obtained from each DEM. The SELNOT procedure of the ANUSPLIN package was used to remove one point from each of the five closest data pairs in three dimensional space, with elevations obtained from the 10 km DEM. Horizontal and elevation coordinates were each scaled to have unit variance. The IDs of the removed points were almost the same as the first five removed

in the two dimensional analysis in the companion paper. They were also very similar to points selected in the same way using elevations from the other DEMs. They were, in order of removal, 341, 37, 369, 192, 378. The remaining 95 points are plotted in Figure 2 together with elevation contours of the 10 km resolution DEM.

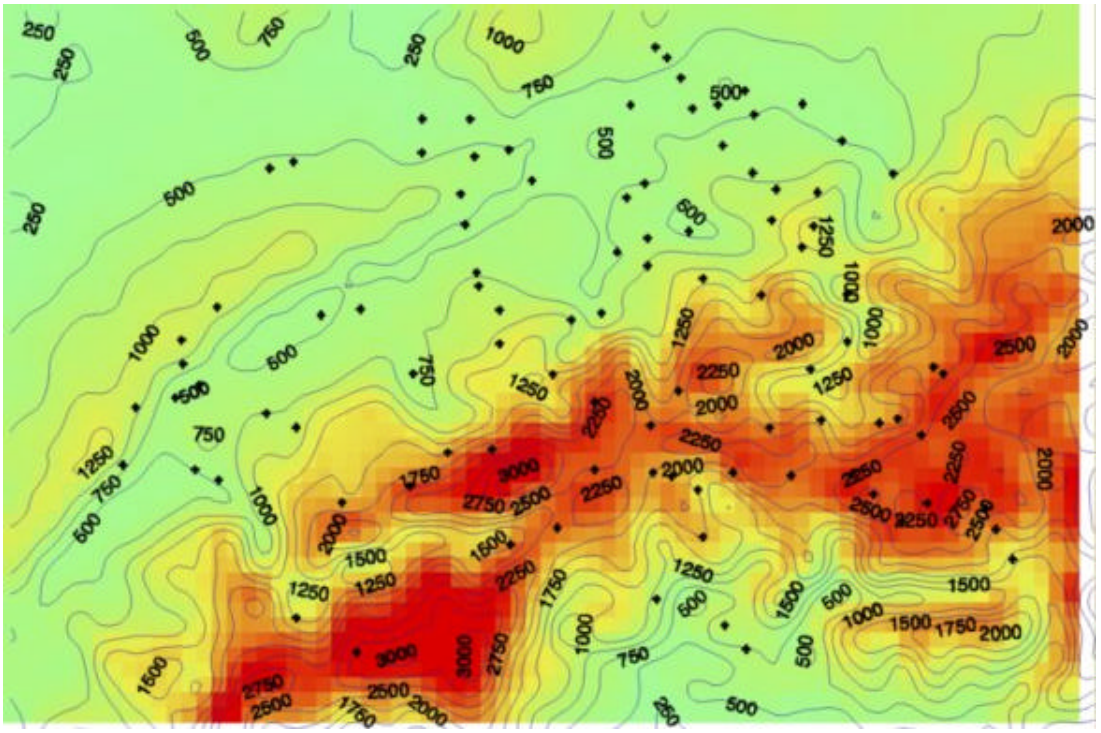

Figure 2 Contour plot of the 10 km resolution DEM overlaid with positions of the 95 data points selected for detailed analysis.

Since generalized cross validation (GCV) was unlikely to be completely reliable in selecting and calibrating different spline models, due to the small size of the data set and the short range correlation evident in the data, an additional five points were withheld from the data set. These were also selected by the SELNOT procedure, as the five points which remain after points were successively removed from the 95 closest data pairs. This is how the SELNOT procedure normally selects knots to evenly sample the three dimensional space spanned by the data points. This procedure was used to select spatially representative withheld data points in the analysis of mean precipitation data by Hutchinson (1995a). The IDs of the points selected here were 13, 102, 138, 357, 466.

The two sets of five removed points were combined into a data set of 10 withheld points. Residuals from these points of spline functions fitted to the remaining 90 points were used, together with the GCV, to guide model selection and calibration, including selection of DEM resolution and optimizing the scale of the elevation dependence.

5. Optimization of DEM resolution and elevation scale

Initial analyses using a second order thin plate spline function of two horizontal coordinates and one elevation coordinate yielded exact interpolation, despite the removal of close data point pairs. The spline order was then increased to three, so that the

roughness penalty defining the nature of the interpolation was calculated in terms of third order derivatives of the fitted function. This yielded stable behaviour as close pairs were removed.

Elevations from the different DEMs were used at different scales in the third order spline analyses. An elevation scaling of 100 times the position coordinates, as has been determined in earlier thin plate spline analyses of precipitation (Hutchinson and Bischof 1983, Hutchinson 1995a) was initially selected. This was achieved by having position coordinates in kilometres and elevation coordinates in decametres (i.e. obtained by dividing metres by 10). Table 2 shows the square root of the GCV and the RMS residual from the 10 withheld data points, as functions of DEM resolution. Both the GCVs and the RMS validation residuals indicated that a resolution of 10 km was appropriate.

Table 2. Statistics of third order thin plate spline functions of station position in km and station elevation in decametres, as obtained from DEMs of different resolutions, fitted to 90 selected square root rainfall values.

DEM Resolution (km)	Square Root GCV ($mm^{1/2}$)	RMS Residual from 10 withheld data points ($mm^{1/2}$)
2.5	0.725	2.306
5	0.785	1.555
8	0.656	1.592
10	0.611	1.315
20	0.643	1.414

A similar analysis of elevation scaling was performed, using different scalings of elevations obtained, now from just the 10 km resolution DEM. The GCV and RMS validation residuals confirmed the decameter scaling of elevation.

6. Model selection

Using elevations from the 10 km DEM scaled in decameters, and position coordinates in km, several spline models, including the models examined by Hutchinson (1995a), were fitted to the 90 selected data points. In each case the degree of data smoothing was determined by minimizing the GCV. The types of spline models considered in this paper are listed in Table 3.

Table 3. Types of spline models. Horizontal coordinates are denoted by x,y. Elevation is denoted by h. The eastern and northern components of the unit normal vector to the 10 km resolution vertically exaggerated DEM are denoted by p and q respectively. Spline functions are denoted by f. Fitted constants are denoted by a and b.

Model ID	Functional form	Description
A	$f(x,y)$	Bivariate thin plate spline
B	$f(x,y) + ah$	Trivariate partial thin plate spline
C	$f(x,y,h)$	Trivariate thin plate spline
D	$f(x,y,h) + ap + bq$	Quintvariate partial thin plate spline
E	$f(x,y,p,q)$	Quartvariate thin plate spline

Model A denotes a bivariate spline function with no topographic dependence. Model B denotes a trivariate partial spline function with a constant dependence on elevation.

Model C denotes a trivariate spline function with a spatially varying dependence on elevation. This spline model is commonly used to model monthly mean precipitation and temperature (Hutchinson and Bischof 1983, Hutchinson 1991).

Model D denotes a quintvariate spline function with a spatially varying dependence on elevation and a constant dependence on the two components of the unit normal vector to the 10 km resolution DEM, as given by equations (1,2) above. Model E denotes a quartvariate spline function with a spatially varying dependence on DEM slope and aspect but no explicit dependence on elevation. Model E was not applied to the initial small data set. The two components of the unit normal vector were calculated from the same vertically exaggerated DEM used to provide the station elevations. This increases the relative orographic effect of smaller slopes.

Results of the initial analyses using these models, with various orders, are shown in Table 4. As reported in the companion paper, the third order bivariate spline was inferior to the second order bivariate spline. Not surprisingly, in view of Figure 1(b), a partial spline dependence on elevation did not yield a significant improvement over the second order bivariate spline.

Table 4. Statistics of smoothing spline analyses of 90 selected data points with RMS residuals from 10 withheld data points. The types of splines are indicated by the model IDs defined in Table 3.

Model ID	Order of spline	Signal	Square root of GCV ($mm^{1/2}$)	Estimate of standard deviation of model error ($mm^{1/2}$)	RMS residual from 10 withheld data points ($mm^{1/2}$)
A	2	78.4	0.740	0.266	0.854
A	3	54.4	0.762	0.480	1.393
B	2	78.4	0.748	0.268	0.841
C	2	90.0	0.655	0.0	0.708
C	3	71.9	0.611	0.274	1.315
D	3	71.6	0.585	0.265	1.160

The second order trivariate spline failed to produce any data smoothing, and was therefore rejected, although both the GCV and the RMS validation residual suggested good predictive performance. The third order quintvariate partial spline was selected for further analysis, since both the GCV and the RMS validation residual were marginally smaller than the corresponding statistics for the third order trivariate thin plate spline. There were conflicting indications of the predictive performance of this model in relation to the predictive performance of the second order bivariate spline model. The GCV suggests that the quintvariate model is superior, while the RMS residual suggests that the bivariate spline is superior.

The fitted constants for the quintvariate partial spline were a = -0.24 and b = -0.21. These indicated a south western aspect effect on precipitation, with greater precipitation on south western facing slopes and less precipitation on north eastern facing slopes. This was verified by referring to the upper atmosphere winds above Payerne on the north western edge of the Alps. From 7 May to 8 May the wind direction above this station at the 700 hPa and 500 hPa levels moved slowly from the south, through south west, to the west (Swiss Meteorological Institute, pers. comm.).

The quintvariate partial spline model was assessed in detail by applying it to the 95 data points shown in Figure 2, consisting of all data points except those points removed from the five closest pairs, as described above. Thus the five representative points chosen above were returned to the analysis. The statistics for this model were quite similar to the statistics for the same model applied to the 90 selected data paints. The signal for this model was 76.5, the square root GCV was 0.593 $mm^{1/2}$ and the estimated standard deviation of the model error was 0.261 $mm^{1/2}$. The coefficients of the two components of the unit normal to the vertically exaggerated 10 km DEM were a = -0.23 and b = -0.22, with standard errors of 0.09 and 0.08 respectively. These standard errors were estimated using the method described in Hutchinson (1993).

7. Statistics

Most statistics and maps are presented in terms of the square root analysis and for the ensuing untransformed values, obtained by simply squaring all interpolated square root rainfall values. Standard errors for the untransformed interpolated values were calculated using equation (3) of the companion paper (see Hutchinson 1998). All rainfall values are in units of mm and all square root rainfall values are in units of $mm^{1/2}$.

General statistics are presented in Table 5 and histograms of all 467 estimated values are shown in Figure 3. These indicate close agreement with the means, slight reduction of the medians and slight increase in standard deviation. The incorporation of topographic dependence has plainly added variability. This is also indicated in the histograms of the interpolated values shown in Figure 3, which show more variability than the data histograms shown in Figure 1 of the companion paper (see Hutchinson 1998).

Table 5. General statistics for the withheld 367 data points and for the 367 estimated values.

Data	Minimum	Maximum	Mean	Median	Standard deviation
True square root values ($mm^{1/2}$)	0	7.19	4.07	4.02	1.39
Estimated square root values ($mm^{1/2}$)	0	7.64	4.06	3.87	1.56
True untransformed values (mm)	0	51.7	18.5	16.2	11.1
Estimated untransformed values (mm)	0	58.3	18.9	14.9	12.3

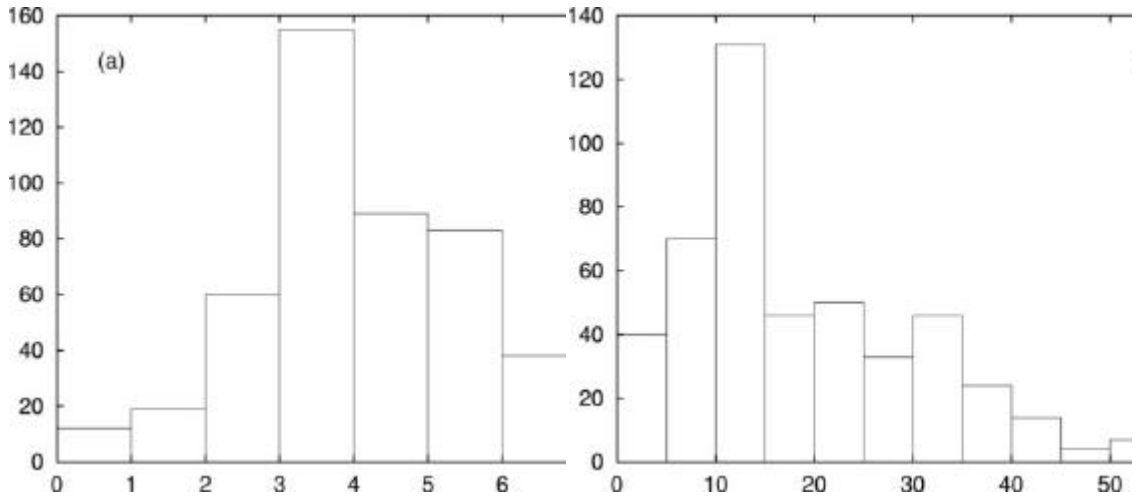

Figure 3. Histograms of (a) interpolated square root values and (b) squared interpolated square root values, for all 467 data points.

Comparative statistics, including the number of agreements with the actual 10 smallest and largest values, are presented in Table 6. Scatter plots of residuals and fitted values for the 367 untransformed data values are shown in Figure 4.

The bias in the square root and untransformed values is negligible. Correlation between data residuals and data values is just -0.22, half of the correlation for the bivariate spline analysis described in the companion paper. Similarly the correlation between the fitted values and the data values is 0.76, significantly less than the correlation for the bivariate analysis.

Table 6. Comparative statistics for the 367 square root and untransformed rainfall data. The number of agreements with the 10 smallest and 10 largest points of all 467 data points.

Data	RMS Error	Bias	Mean Absolute Error	Mean Relative Error	Number in 10 smallest	Number in 10 largest
Square root ($mm^{1/2}$)	0.969	-0.01	0.70	0.20	7	1
Untransformed (mm)	8.14	+0.4	5.7	0.38		

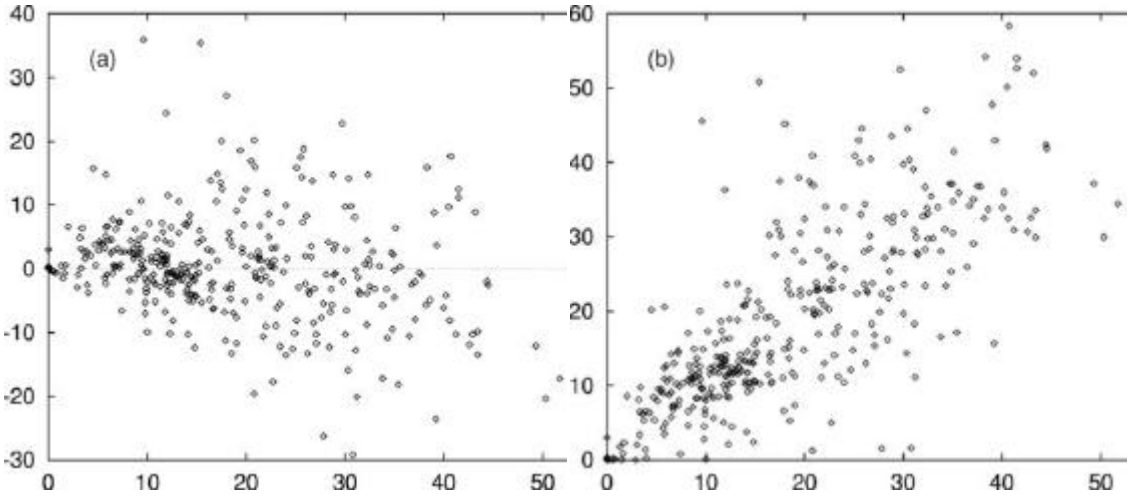

Figure 4 Scatter plots for the 367 withheld values: (a) untransformed data residuals versus data values (correlation = -0.22), (b) fitted untransformed values versus data values (correlation = 0.76).

8. Error map for the square root rainfall values

An isoline plot of the grid of standard errors of the interpolated square root values is shown in Figure 5. This grid is calculated by the ERRGRD program, according to the method for estimating spatially distributed errors described in Hutchinson (1993). This required prior calculation of grids of the eastern and northern components of the unit normal to the 10 km resolution DEM, with elevation units in decameters. The map is clearly related to both station density and the topography shown in Figure 2. The largest estimated standard errors occur at the highest elevations and at positions well beyond the data network.

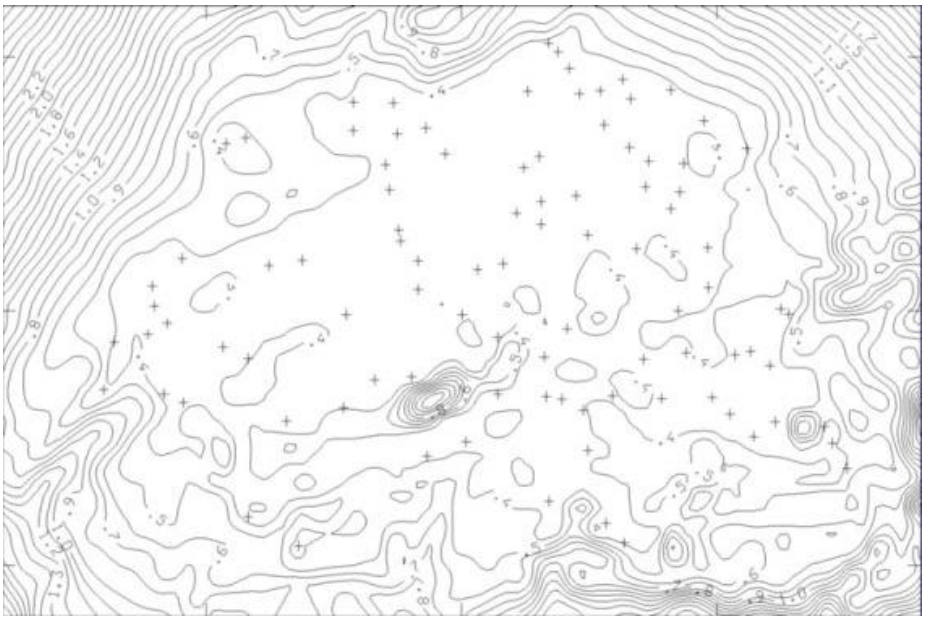

Figure 5 Estimated standard errors for the interpolated square root values ($mm^{1/2}$) overlaid with the positions of the 95 data points used to fit the surface.

9. Maps for the untransformed rainfall values

A proportional symbol map of the untransformed data residuals is shown in Figure 6, overlaid with an isoline plot of the grid of standard errors of the interpolated untransformed rainfall values. This grid is calculated as in the companion paper, with grid values and isolines limited to those grid values for which the estimated standard errors in Figure 5 do not exceed 0.9 $mm^{1/2}$. Interpolated values larger than the observed values are indicated by a cross and interpolated values less than the measured values are indicated by a circle. The size of the residuals are in agreement with the plotted standard error isolines, which now reflect topography, as well as data network density and the magnitude of the interpolated rainfall.

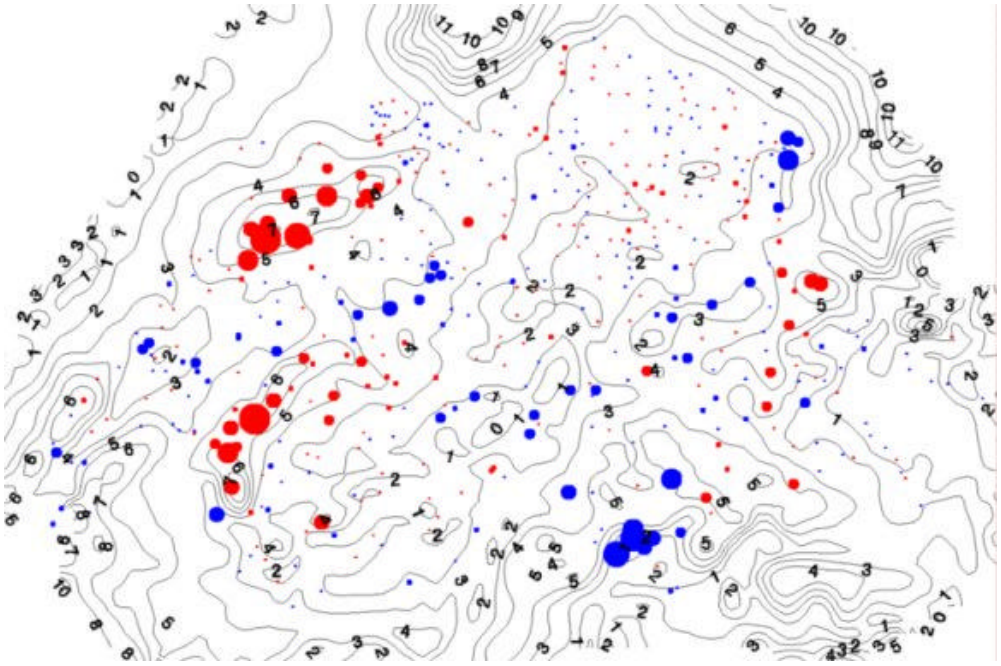

Figure 6 Proportional symbol map of untransformed data residuals, overlaid with isolines of estimated standard errors (mm).

Figure 7 shows an isoline plot of the grid of interpolated untransformed rainfall values, overlaid with the symbols denoting the 10 smallest and 10 estimated largest rainfall data values. This grid was calculated by simply squaring the interpolated square root values. The 10 smallest values are in good agreement with the plotted isolines. The 10 largest values show less agreement, again as for the bivariate analysis.

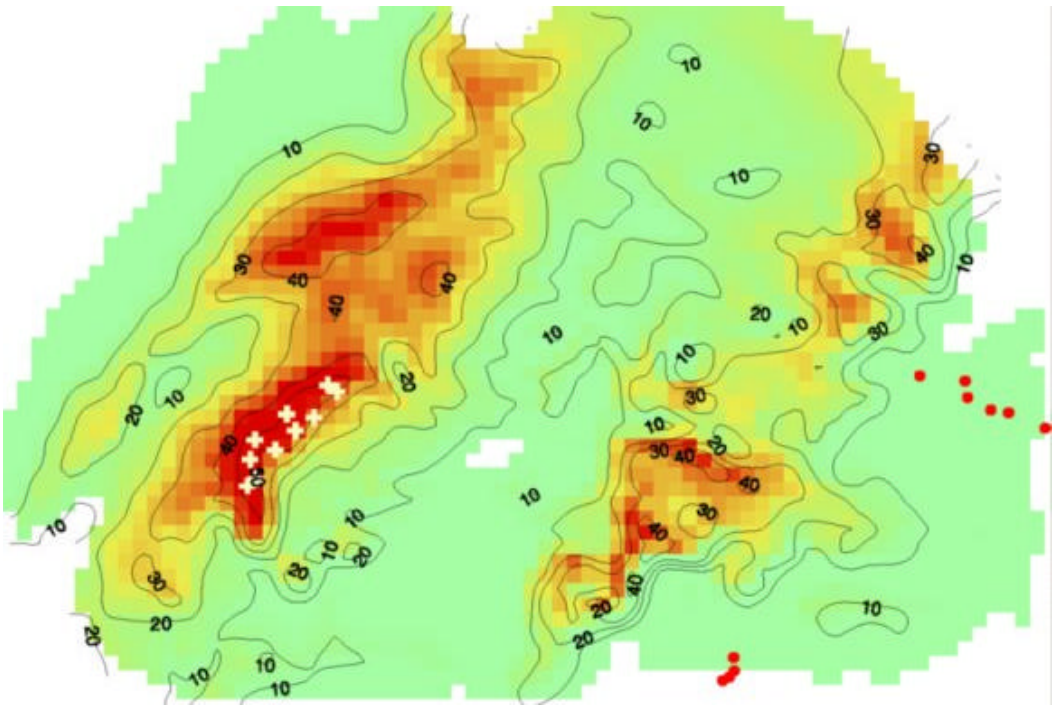

Figure 7 Isolines of the interpolated untransformed values (mm), overlaid with the 10 smallest and 10 largest estimated rainfall data values.

Interpolated rainfall values exceeding 40 mm in the western half of Figure 7 indicate rainfall enhancement by elevation, associated with the Jura Mountains and the north western foothills of the Alps. Interpolated rainfall values exceeding 30 mm in the eastern half of Figure 7 are associated with south western facing slopes to the north of Lake Maggiore and inter alpine valleys associated with the Rhine and Inn Rivers.

The largest positive residuals, indicated by large red dots in Figure 6, appear to be associated with a rain shadow effect south east of the Jura Mountains and a too large elevation enhancement of precipitation on the north western face of the Alps. Similarly, the largest negative residuals, indicated by large blue dots in Figure 6, appear to be associated with a too strong decrease of precipitation with lower elevation north of Lake Maggiore.

10. Interpolation accuracy and performance

As in the companion paper, the accuracy of the interpolated values has been assessed by calculating the standard error estimates plotted in Figure 6 and comparing them graphically with the data residuals. The accuracy and performance of the quintvariate partial spline analysis is slightly less than the accuracy and performance of the bivariate spline analysis. This can be attributed to the lack of strong topographic dependence in this particular data set, and insufficiently many data points to adequately calibrate topographic dependencies. Both analyses found the same regions with the largest and smallest estimated values.

To more closely examine topographic dependencies, and to validate the model selection procedure used above, the roles of the 100 data selected data points and the

withheld 367 data points were reversed. Thus various partial spline models were fitted to the 367 data points and the 100 data points were used for validation. Table 7 documents the performance of these models. The quintvariate partial spline (model D) found the same SW aspect effect, as found by the initial quintvariate analysis, but the two most accurate models were a second order, three dimensional thin plate spline function of position and elevation (model C), and a third order, four dimensional thin plate spline function of horizontal position and the two components of the unit normal vector to the 10 km DEM (model E). The GCVs and RMS validation residuals show strong agreement with the analyses listed in Table 4. With the exception of the second order trivariate spline, all models gave similar estimates for the standard deviation of model error (the nugget standard deviation). The analyses also verified the optimisations of DEM resolution and elevation scale described above.

Table 7. Statistics of smoothing spline analyses of 367 selected data points with RMS residuals from 100 withheld data points. The types of spline models are indicated by the model IDs defined in Table 3.

Model ID	Order of spline	Signal	Square root of GCV ($mm^{1/2}$)	Estimate of standard deviation of model error ($mm^{1/2}$)	RMS residual from 100 withheld data points ($mm^{1/2}$)
A	2	157	0.507	0.384	0.704
A	3	110	0.511	0.359	0.822
B	2	150	0.496	0.382	0.722
C	2	367	0.469	0.0	0.653
C	3	200	0.506	0.341	0.765
D	3	201	0.509	0.342	0.763
E	3	202	0.531	0.356	0.647

Contour lines of the fitted mode E are shown in Figure 8, overlaid with the positions of the actual 10 smallest and 10 largest rainfall values. This analysis shows a pattern more closely aligned with topographic structure than the bivariate analysis in Figure 9 of the companion paper. It also models spatially varying topographic slope and aspect effects on precipitation which are missing from the analysis in Figure 7. It shows enhancement of precipitation in the alpine foothills below elevations of 1500 metres, with precipitation enhanced on southern facing slopes in the south, and precipitation enhanced on western and north western facing slopes to the North West. These effects are in keeping with the directions of the upper atmosphere winds reported above and the strong topographic forcing associated with the Alps. These are also in close agreement with the topographic effects reported in the precipitation climatology produced by Frei and Schar (1998). The analysis afforded by model E provides an alternative to precipitation analyses based on topographic aspect presented by Daly *et al.* (1994).

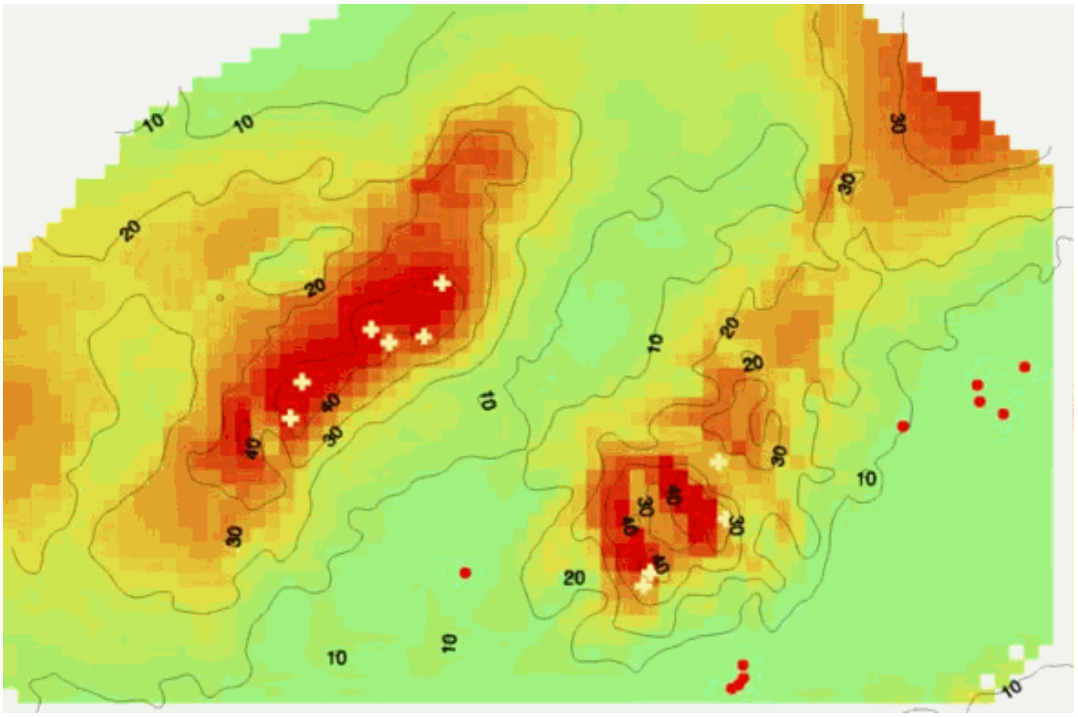

Figure 8 Quartvariate thin plate spline analysis of the 367 data points, overlaid with the positions of the 10 smallest and 10 largest measured rainfall values.

Such higher dimensional analyses are only possible with a larger data set. The larger GCV associated with this analysis is probably a reflection of the larger number of boundary points associated with higher dimensional analyses.

The determination of the SW aspect effect by Model D was quite sensitive to DEM resolution. The effect was lost for DEMs with resolution finer than 10 km. On the other hand model C, which depends on elevation but not aspect, was more robust with respect to DEM resolution, with similar performance for the 8 km and 10 km resolution DEMs.

11. Conclusion

The analyses have illustrated the flexibility of thin plate spline analyses, permitting rapid assessment of a large number of candidate models. The analyses also show that small data sets can be used to reliably calibrate topographic dependencies, despite problems associated with short range correlation and the small size of the data set. The diagnostics associated with thin plate splines assisted these assessments. The analyses also permitted assessment of DEM resolution and elevation scale, an essential first step in calibrating topographic dependencies. The analyses are feasible in emergency situations, especially if a standard DEM resolution and a standard elevation scale are assumed. The elevation scale value optimised from the data in this case was in agreement with previous experience.

The analyses confirmed the importance of incorporating spatially varying topographic dependencies when analyzing rainfall fields. In particular, fitting a constant linear dependence on elevation performed no better than bivariate analyses independent of topography. The equal accuracy of the models which had just a spatially varying

dependence on elevation, or just a spatially varying dependence on slope and aspect, indicates that there is room for further investigation of these topographic dependencies.

It should be kept in mind that this analysis was for just one day of rainfall data, and that the topographic dependence of this data set is relatively small. Different synoptic conditions give rise to rainfall patterns which may contain different topographic dependencies. In particular the elevation dependence of convective and frontal rainfall is known to differ markedly. Moreover, the absence of many zero rainfall data values in this data set, and the dense data network, both significantly aided the analyses. Hutchinson (1995b) has argued the case for an anomaly approach to rainfall interpolation when data are relatively sparse, using historical data to aid in determining topographic dependencies.

References

Barry, R. G. (1981) *Mountain Weather and Climate*. Methuen, London.

Bates, D., Lindstrom, M., Wahba, G. and Yandell, B. (1987) GCVPACK - routines for generalized cross validation. *Communications in Statistics B - Simulation and Computation,* 16: 263-297.

Daly, C., Neilson, R.P. and Phillips, D. L. (1994) A statistical-topographic model for mapping climatological precipitation over mountainous terrain. *Journal of Applied Meteorology,* 33: 140-158.

Frei, C. and Schar, C. (1998) A precipitation climatology of the Alps from high-resolution rain-gauge observations. *International Journal of Climatology,* 18: 873-900.

Hutchinson, M. F. (1991) The application of thin plate smoothing splines to continent-wide data assimilation. In: *Data Assimilation Systems*, edited by J. D.Jasper, BMRC Research Report No.27, pp. 104-113. Melbourne: Bureau of Meteorology.

Hutchinson, M. F. (1993) On thin plate splines and kriging. In: *Computing and Science in Statistics, Vol. 25.* Edited by M.E.Tarter and M.D.Lock, pp. 55-62. Berkeley: Interface Foundation of North America.

Hutchinson, M. F. (1995a) Interpolation of mean rainfall using thin plate smoothing splines. *International Journal of Geographical Information Systems,* 9: 385-403.

Hutchinson, M. F. (1995b) Stochastic space-time weather models from ground-based data. *Agricultural and Forest Meteorology,* 73: 237-264.

Hutchinson, M. F. (1996) A locally adaptive approach to the interpolation of digital elevation models. *Third International Conference/Workshop on Integrating GIS and Environmental Modeling, Santa Fe, NM, January 21-26*, (1996. Santa Barbara: National Center for Geographic Information and Analysis.
http://www.ncgia.ucsb.edu/conf/SANTA_FE_CD-ROM/main.html.

Hutchinson, M. F. (1997a) *ANUSPLIN Version 3.2*,
http://cres.anu.edu.au/software/anusplin.html..

Hutchinson, M. F. (1997b) *ANUDEM Version 4.6*,
http://cres.anu.edu.au/software/anudem.html.

Hutchinson, M. F. (1998) Interpolation of rainfall data with thin plate smoothing splines: I Two dimensional smoothing of data with short range correlation, ftp://ftp.geog.uwo.ca/SIC97/Hutchinson_1/Hutchinson_1.html

Hutchinson, M. F. and Bischof, R. B. (1983) A new method for estimating mean seasonal and annual rainfall for the Hunter Valley, New South Wales. *Australian Meteorological Magazine*, 31: 179-184.
Hutchinson, M. F. and Gessler, P. E. (1994) Splines - more than just a smooth interpolator. *Geoderma,* 62: 45-67.
Wahba, G. (1990) *Spline models for Observational Data*. CBMS-NSF Regional Conference Series in Applied Mathematics. Philadelphia: Society for Industrial and Applied Mathematics.

JGIDA vol. 2, no. 2
JGIDA Home